PRP Pharmacology Research & Perspectives
Open Access

ORIGINAL ARTICLE

Clearance of systemic hematologic tumors by venetoclax (Abt-199) and navitoclax

Scott Ackler[a], Anatol Oleksijew[a], Jun Chen, Brenda J. Chyla, Jerry Clarin, Kelly Foster, Thomas McGonigal, Sasmita Mishra, Sally Schlessinger, Morey L. Smith, Stephen K. Tahir, Joel D. Leverson, Andrew J. Souers, Erwin R. Boghaert & Jonathan Hickson

AbbVie Inc., North Chicago, Illinois

Keywords
Apoptosis, Bcl-2 family proteins, bioluminescent imaging, drug therapy, leukemia/lymphoma, systemic engraftment

Correspondence
Scott Ackler, AbbVie Inc., Building AP9/2185, 1 North Waukegan Road, North Chicago, 60064 IL. Tel: 847 935 1792;
Fax: 847 937 4150;
E-mail: scott.ackler@abbvie.com

Received: 12 March 2015; Revised: 23 July 2015; Accepted: 3 August 2015

Pharma Res Per, 3(5), 2015, e00178, doi: 10.1002/prp2.178

doi: 10.1002/prp2.178

[a]These authors contributed equally to this work.

Abstract

The Bcl-2 family inhibitors venetoclax and navitoclax demonstrated potent antitumor activity in chronic lymphocytic leukemia patients, notably in reducing marrow load and adenopathy. Subsequent trials with venetoclax have been initiated in non-Hodgkin's lymphoma and multiple myeloma patients. Traditional preclinical models fall short either in faithfully recapitulating disease progression within such compartments or in allowing the direct longitudinal analysis of systemic disease. We show that intravenous inoculation of engineered RS4;11 (acute lymphoblastic leukemia) and Granta 519 (mantle cell lymphoma) bioluminescent reporter cell lines result in tumor engraftment of bone marrow, with additional invasion of the central nervous system in the case of Granta 519. Importantly, apoptosis induction and response of these systemically engrafted tumors to Bcl-2 family inhibitors alone or in combination with standard-of-care agents could be monitored longitudinally with optical imaging, and was more accurately reflective of the observed clinical response.

Abbreviations

ALL, acute lymphoblastic leukemia; BR, bendamustine-rituximab; CLL, chronic lymphocytic leukemia; IHC, immunohistochemistry; IV, intravenous; LM, Cluc2-mCherry; MCL, mantle cell lymphoma; ROI, region of interest; SC, subcutaneous; TGD, tumor growth delay.

Introduction

Bcl-2 is an antiapoptotic protein frequently overexpressed in leukemias and lymphomas. In particular, nodal follicular lymphomas harbor a hallmark t(14;18) translocation, which leads to expression control of Bcl-2 being regulated by the IgH enhancer region, in 60–90% of cases (Tsujimoto et al. 1984; Sekiguchi et al. 2005). Bcl-2 overexpression is frequently observed in hematologic tumors even in the absence of this translocation, and is associated with increased mortality and rate of relapse (Wei 2004). Navitoclax (ABT-263) and venetoclax (ABT-199) (structures in Fig. S1) are small molecule inhibitors of the antiapoptotic Bcl-2 family proteins designed to restore proper apoptotic homeostasis. Navitoclax inhibits family members Bcl-2, Bcl-x_L, and Bcl-w (Tse et al. 2008), specifically activating the intrinsic apoptotic cascade. Venetoclax, an inhibitor which specifically targets Bcl-2, demonstrates similar target-driven activity, is significantly more potent than navitoclax, and the absence of Bcl-x_L binding makes this agent platelet sparing (Souers et al. 2013).

In subcutaneous (SC) xenograft models, these inhibitors have demonstrated single agent antitumor efficacy against multiple leukemia and lymphoma cell types (Lock et al. 2008; Tse et al. 2008; Souers et al. 2013), and in vivo potentiation has been seen with other chemotherapeutic agents and regimens (Tse et al. 2008; Ackler et al.

2010, 2012; Souers et al. 2013). In contrast, intravenous (IV) inoculation of cancer cells via the tail vein allows dissemination throughout the animal and seeding to the organ(s) of preference. The major advantage of these models over SC inoculation is that growth in these conditions closely mimics human disease by allowing for proper microenvironmental interaction and engraftment in clinically relevant sites. Monitoring tumor growth and disease progression in these models can be cumbersome, involving serial bleeding, and analysis for specific markers (i.e., CD45) or relying on clinical observations of moribundity as an end point (Liem et al. 2004).

To determine preclinical activity of Bcl-2 inhibitors in systemic disease, we employed in vivo optical imaging. This technology has been used over the past decade to noninvasively track cancer cells stably expressing bioluminescent and/or fluorescent reporters longitudinally to accurately monitor tumor growth in ectopic, orthotopic, metastatic, or systemic models (Kaijzel et al. 2007; Weissleder and Pittet 2008; Hickson 2009; O'Neill et al. 2010). We induced stable expression of the fusion construct of luc2, a firefly luciferase optimized for expression in mammalian cells, and mCherry, a far red fluorescent protein (luc2-mCherry or LMC hereafter), in an acute lymphoblastic leukemia (ALL) cell line, RS4;11 and a mantle cell lymphoma (MCL) cell line, Granta 519. We report consistent systemic engraftment in bone marrow of both models, with additional invasion of the central nervous system in the case of Granta 519-LMC. Bioluminescence was utilized to monitor cancer growth as well as response to navitoclax, venetoclax, and standard chemotherapy agents. We also evaluated the rapid pharmacodynamic induction of apoptosis in tumors following treatment with Bcl-2 inhibitors using both classical immunohistochemical (IHC) approaches and the novel bioluminescent probe VivoGlo.

Materials and Methods

Cell culture

RS4;11 and Granta 519 cells were purchased from Deutsche Sammlung von Mikroorganismen und Zellkulturen GmbH (Braunschweig, Germany). Cells were cultured in RPMI 1640 media (Invitrogen, Carlsbad, CA) supplemented with 10% fetal bovine serum (FBS) (Hyclone, Logan, UT) and maintained at 37°C in 5% CO_2 and 95% relative humidity.

Vector construction and cell line generation

A fusion construct of luc2 (Promega, Madison, WI) and mCherry (Clontech, Mountain View, CA) was cloned into the Lenti-X lentiviral vector (Clontech). Cells were transduced with lentiviral particles for 48 h and a pool of cells stably expressing the fusion construct were selected using 2 $\mu g \cdot mL^{-1}$ puromycin for 2 weeks.

Reagents

D-luciferin, VivoGlo reagent, and goat anti-luciferase antibody were purchased from Promega. Navitoclax and venetoclax were synthesized at AbbVie as previously described (Park et al. 2008; Souers et al. 2013). Cyclophosphamide was purchased from Bristol-Myers Squibb (Princeton, NJ). Doxorubicin was purchased from Bedford Laboratories (Bedford, OH). Vincristine was purchased from Mayne Pharmaceuticals (Paramus, NJ). Prednisolone was purchased from ETHEX Corp (St Louis, MO). Bendamustine was purchased from Cephalon Inc (Frazer, MA). Rituximab was purchased from Genentech (South San Francisco, CA). Phosal 50 PG was purchased from American Lecithin (Oxford, CT). Rabbit anti-cleaved caspase 3 antibody was purchased from Cell Signaling (Danvers, MA).

In vitro analysis

To determine in vitro photon flux, RS4;11-LMC or Granta 519-LMC cells were plated at different densities in 96-well plates. 150 μmol/L D-luciferin was added to each well and luciferase activity was measured with a Xenogen IVIS Spectrum Imaging system (Perkin Elmer, Waltham, MA). Luminescent signal (photons/s) for each well was quantified using Living Imaging 4.0 (Perkin Elmer) and plotted as average values versus cell number. Photon flux was calculated as the slope of the line. Sensitivity to navitoclax and venetoclax was determined following 48 h exposure. Viability was assessed using CellTiter-Glo (Promega), with luminescence measured on an SpectraMax M5 spectrophotometer (Molecular Devices, Sunnyvale, CA). IC_{50} curves were plotted using GraphPad Prism5 (La Jolla, CA).

Mouse in vivo experiments

C.B. -17 *scid*-bg mice were purchased from Charles Rivers Laboratories (Wilmington, MA). About 8 to10 mice were housed per cage. Body weights upon arrival were 18–20 g. Food and water were provided ad libitum. Mice were acclimatized to the animal facilities for at least 1 week prior to inoculation. Animals were tested in the light phase of a 12 h light:12 h dark cycle (lights on at 06:00 h). All animal studies were conducted in accordance with the guidelines established by the AbbVie Institutional Animal Care and Use Committee and the

National Institutes of Health Guide for Care and Use of Laboratory Animals guidelines in a facility accredited by the Association for the Assessment and Accreditation of Laboratory Animal Care. The total number of mice used in the present experiment was approximately 500. Temperature was maintained at 25°C. All studies involving animals are reported in accordance with the ARRIVE guidelines (Kilkenny et al. 2010; McGrath et al. 2010).

For flank xenograft trials, mice were inoculated with 5×10^6 RS4;11-LMC or Granta 519-LMC cells subcutaneously in a 0.2 mL inoculum of a 1:1 mixture of cells in culture media and Matrigel (BD Biosciences, Bedford, MA). Tumor volume was estimated by 2–3 weekly measurements of the length and width of the tumor by electronic calipers and applying the following equation: $V = L \times W^2/2$. When tumors reached approximately 250 mm^3, the mice were size-matched (day 0) into treatment and control groups. All treatment groups consisted of 10 mice per group. Tumor growth delay (%TGD) was calculated as previously described (Souers et al. 2013).

For systemic engraftment studies, 2×10^6 cells were inoculated intravenously in a 0.2 mL volume of culture media on day 0. Disease progression was monitored via in vivo bioluminescent imaging (see below). Animals were staged at approximately 14 days (Granta 519-LMC) or 21 days (RS4;11-LMC) following inoculation by inclusion of animals within a range of the median of whole-body region-of-interest (ROI) coupled with detectable bone marrow involvement. Further measurements monitoring tumor burden were analyzed by whole-body ROI. Animals were euthanized when a bioluminescence (BLI) signal of 1×10^9 (RS4;11-LMC) or 2×10^8 (Granta 519-LMC) was achieved or when the animals demonstrated distress. BLI values of 5×10^8 and 1×10^8 were used as endpoint calculations for %TGD in RS4;11-LMC and Granta 519-LMC, respectively. Unless otherwise stated, all experiments were performed with eight mice per treatment group.

Immunohistochemistry

All tissues and tumors were harvested and fixed for approximately 48 h in 10% neutral buffered formalin. Bone samples were decalcified using Immunocal (Decal Chemical, Tallman, NY) for 8–24 h depending upon size and bone density. Other tissues were routinely processed, and blocks were sectioned at 5 μm. Goat anti-luciferase was used at a dilution of 1:1000, and rabbit anti-cleaved caspase 3 at a dilution of 1:100. Secondary detection was performed using either goat on rodent horseradish peroxidase (HRP)- polymer (Biocare Medical, Concord, CA) or rabbit Envision Plus–HRP polymer (Dako, Carpenteria, CA), with 3,3′-diaminobenzidine as a chromogen.

Statistical analysis

Significance within caspase activation experiments was performed by two-tailed Student's *t*-test. Significance for %TGD was performed by Kaplan Meier log rank analysis. $P < 0.05$ was considered significant.

Results

RS4;11 and Granta 519 cells with stable expression of a fused bioluminescent and fluorescent reporter gene retain sensitivity to venetoclax and navitoclax

The LMC cassette was spliced into the Lenti-X lentiviral vector for transduction of RS4;11 ALL and Granta 519 MCL cells. Transduced cells were selected using puromycin, and the resulting pool stably expressing the construct (referred to as RS4;11-LMC and Granta 519-LMC) were determined to have an in vitro photon flux of 150 and 72 photons $\cdot$ $cell^{-1}$, respectively (Fig. 1A and B). To ensure that the selected cells did not have altered response rates to navitoclax and venetoclax, sensitivity of RS4;11-LMC and Granta 519-LMC were compared to the sensitivity of their respective parent line. Response curves were indistinguishable between parental and LMC lines (Fig. 1C and D). RS4;11-LMC was further characterized in vivo, and SC xenografts treated with navitoclax or venetoclax (Fig. 1E), demonstrating similar sensitivity as the parental line (Tse et al. 2008; Souers et al. 2013). We have previously demonstrated that navitoclax and venetoclax monotherapy are only weakly active in Granta 519 SC xenografts (Tse et al. 2008; Souers et al. 2013). Therefore, these agents were tested in combination with bendamustine and rituximab (BR) which have demonstrated strong combinatorial activity with Bcl-2 inhibitors preclinically (Ackler et al. 2012). Granta 519-LMC responded similarly to the parent cell line when treated with BR alone or in combination with navitoclax or venetoclax (Ackler et al. 2012; Souers et al. 2013) (Fig. 1F).

Molecular imaging of apoptosis induction by Bcl-2 inhibition in SC RS4;11-LMC xenografts

Previously, we have demonstrated the ability of VivoGlo to accurately and noninvasively visualize caspase activation in vivo (Hickson et al. 2010). VivoGlo is a modified firefly luciferase substrate (Z-DEVD-aminoluciferin) that is cleaved and activated by caspases 3/7 to liberate aminoluciferin, which can then be consumed by luciferase to generate a luminescent signal. Because the function of

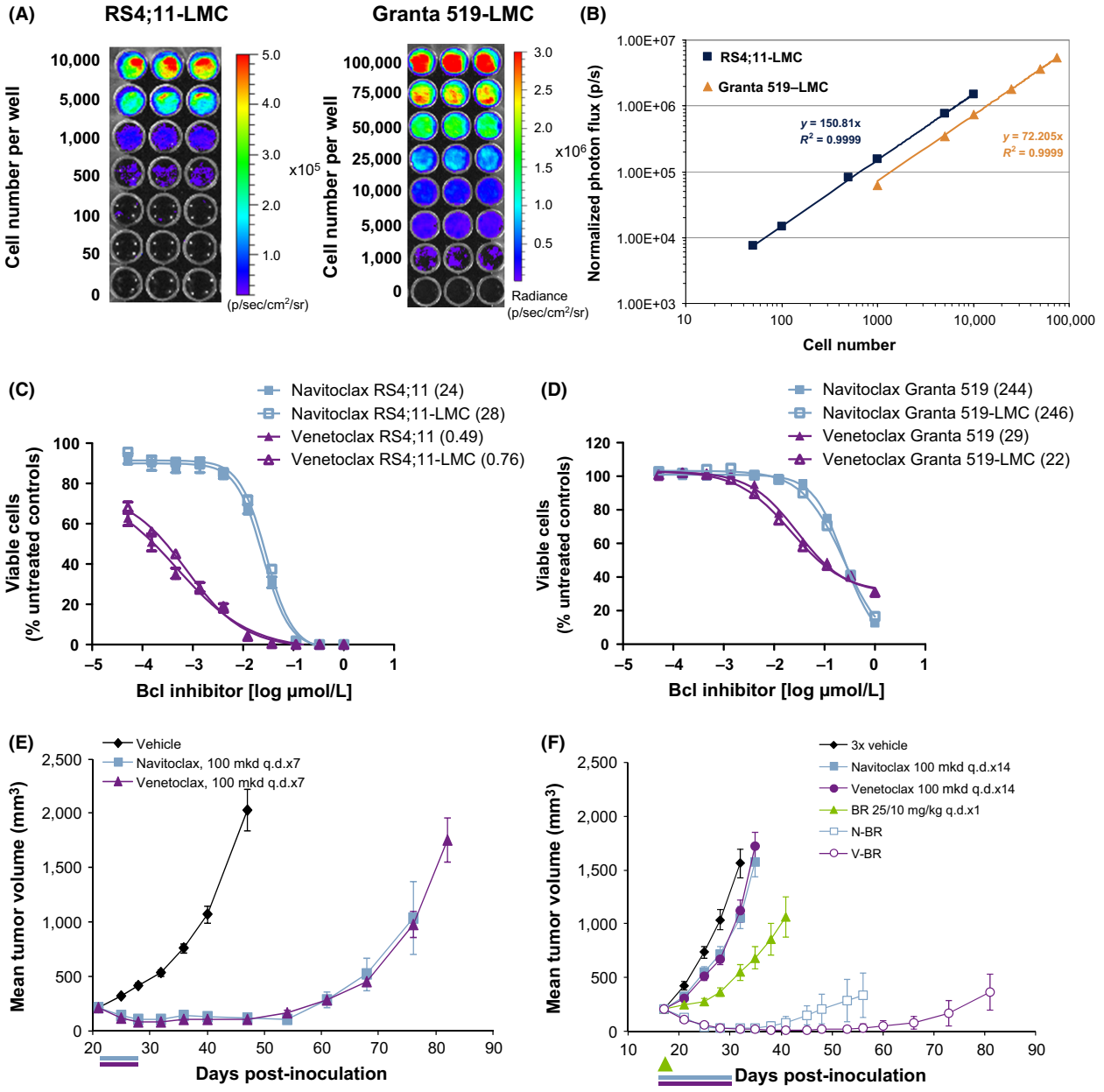

Figure 1. Generation and characterization of RS4;11-LMC and Granta 519-LMC. (A) In vitro photon flux analysis of RS4;11-LMC and Granta 519-LMC. Cells were plated at the densities shown. (B) Graphical representation of photon flux data for RS4;11-LMC and Granta 519-LMC. Photon flux is calculated as the slope of the line, shown in the inset. (C and D) Comparison of in vitro response curves for navitoclax and venetoclax in RS4;11 and RS4;11-LMC, and Granta 519 and Granta 519-LMC, as measured using CellTiterGlo. Response curves presented as mean ± SEM of three replicates. IC_{50} values in nmol/L are shown in legends in parentheses. (E) RS4;11-LMC flank xenograft tumors treated with either vehicle, navitoclax, or venetoclax (100 mg·kg^{-1}·day^{-1}, p.o. q.d. × 7). (F) Granta 519-LMC flank xenografts treated with either vehicle, navitoclax, or venetoclax (100 mg·kg^{-1}·day^{-1}, p.o. q.d. × 7), BR (25, 10 mg·kg^{-1}, q.d. × 1) or BR combined with navitoclax or venetoclax. Bars underneath graphs represent dosing period. For (F), green arrow represents BR administration. *N* = 10 mice per treatment group, data presented as mean ± SEM.

luciferase requires viable cells which produce ATP, D-luciferin consumption was used as a control for viability of the tumor tissue to produce a luminescent signal. IHC was used to confirm caspase activation and the level of necrosis within tumor samples to verify signal from Vivo-Glo and D-luciferin, respectively.

To determine the extent and kinetics of caspase activation induced by navitoclax or venetoclax in RS4;11-LMC

SC tumors, we utilized VivoGlo following a single dose of these agents. Tumor-bearing mice were treated and imaged following administration of VivoGlo at 2, 6, and 24 h, or with D-luciferin at −2 h (predose), 28, and 48 h. These staggered timepoints were chosen to allow for washout of bioluminescent probes prior to subsequent imaging.

Caspase activation is shown in Figure 2A and B. Venetoclax-induced caspase activation more rapidly than navitoclax, with approximately 70% of venetoclax-treated tumor cells staining positive for cleaved caspase 3 after 2 h, as compared to approximately 5% for navitoclax-treated tumors. By 24 h, navitoclax-treated tumors had reached 80% caspase positivity, while caspase staining was seen in 99% of venetoclax-treated tumors. VivoGlo imaging demonstrated increased caspase activity of 1.5-fold and 1.8-fold as early as 2 h following navitoclax or venetoclax treatment, respectively. Decreasing signal strength at 24 h was observed for both cohorts (0.8-fold and 0.1-fold, respectively). However, as the presence of ATP-producing cells expressing luciferase is essential for VivoGlo bioluminescent signal production, Figure 2C and D show H&E staining and D-luciferin signal, respectively. Necrotic cells appeared more rapidly following venetoclax treatment (35% by 2 h, 99% by 24 h) than with navitoclax (5% by 2 h, 80% by 24 h). By 28 h, venetoclax had markedly decreased luciferase activity by 95%, which further diminished to 98% of control signal by 48 h. Similarly, navitoclax also demonstrated a decrease in luciferase signal at 28 h of 61% of control signal that was maintained through 48 h. Normalizing VivoGlo signal to D-luciferin signal demonstrated that navitoclax and venetoclax induce significant apoptosis as early as 2 h, with the percentage of VivoGlo signal as a factor of total signal rising from 6% to 10% and 12%, respectively. Signal ratio, 24 h after dosing revealed further increases in apoptotic signal from 7% for vehicle-treated tumors to 14% and 21% for navitoclax- and venetoclax -treated tumors, respectively (Fig. 2E).

Sites of engraftment following IV inoculation of RS4;11-LMC mirror those in patients

Mice were inoculated IV with 5×10^5 to 2×10^6 RS4;11-LMC cells and bioluminescence was used to track tumor growth longitudinally. Using whole-body ROI to quantify tumor burden, tumor engraftment and growth was rapid, reaching a moribundity endpoint (typically hind limb paralysis) approximately 40 days post-inoculation. Empirically, we determined that a bioluminescent signal of 1×10^9 photons $\cdot$ sec^{-1} was predictive of imminent moribundity, and in all subsequent studies mice were humanely euthanized upon reaching this endpoint. Tumor engraftment rates following IV inoculation were >80%, with highly consistent growth as shown in Figure 3A tracking individual mice. Flow cytometric analysis was performed on whole blood and bone marrow samples from a limited set of mice at 4–5 weeks postinoculation. The presence of RS4;11-LMC cells was detected using antibodies against human CD45 and in contrast to the significant number of tumor cells identified in the bone marrow, only a limited number of these cells were found in circulation at 5 weeks (6.8–32% vs. 0.3–2.0%, respectively, data not shown).

BLI analysis indicated that RS4;11-LMC cells were reproducibly engrafted in both hind legs, within the thoracic cavity (most likely the lung), and abdomen. The abdominal signals, consistent with involvement of the liver and spleen, were observed less frequently (Fig. 3B). H&E staining of decalcified bone revealed significant bone marrow invasion, and changes in bone architecture and morphology. The hematopoietic precursor cells along with stromal cells of bone marrow were replaced and effaced by multifocal tumor masses, and also extended into the surrounding skeletal muscle. The tumor masses were densely populated with uncircumscribed boundaries. The medullary trabecular bones were severely affected with scalloped border and the cortical bones adjacent to the tumor cells showed multiple reversal and resting lines (Fig. 3C). The growth plates of all the affected bones were disorganized with retention of cartilages in the metaphyseal trabecular and cortical compact bones. The presence of tumor cells was confirmed by immunohistochemistry using an anti-luciferase antibody (Fig. 3C). The lungs, liver, and spleen were diffusely infiltrated with individual and small aggregates of tumor cells (Fig. 3D). Tumor growth kinetics were similar for whole-body ROI and legs only ROI (Fig. 3E), demonstrating that growth within the marrow compartment was at a similar rate to other distal sites.

Differential response of RS4;11-LMC to Bcl-2 inhibitors in SC and systemic engraftment models

Efficacy of navitoclax and venetoclax was assessed in the RS4;11-LMC systemic engraftment model. On day 21 post-inoculation, animals were imaged and distributed into treatment groups based on whole-body ROI signal (d0). Treatment was begun the following day and response to therapy was tracked longitudinally. Both navitoclax and venetoclax demonstrated significant efficacy (Fig. 4A), although the durability of the response was more than twofold lower as compared to SC xenografts (Fig. 1E). Chemotherapeutics cyclophosphamide and ben-

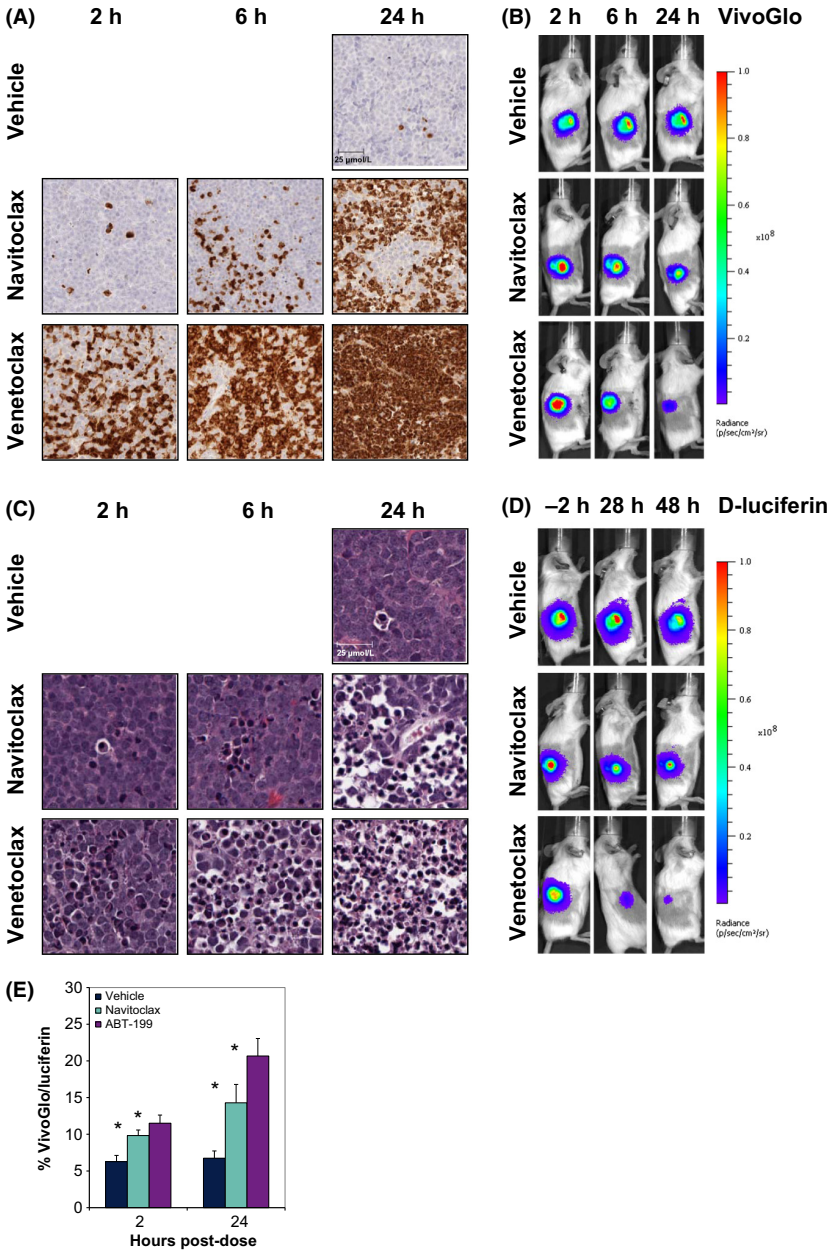

Figure 2. In vivo validation of VivoGlo in RS4;11 flank xenograft tumors. (A) Staining for cleaved caspase-3/7 in RS4;11-LMC following a single dose of navitoclax or venetoclax at 100 mg·kg^{-1}. Pictures are representative images for each timepoint ($N = 3$). Scale bar represents 25 μm, presented in the vehicle-treated group. (B) Representative images of VivoGlo bioluminescence in mice bearing flank xenograft RS4;11 flank tumors treated with either vehicle, navitoclax (100 mg·kg^{-1}), or venetoclax (100 mg·kg^{-1}). Images were taken at 2, 6, and 24 h posttreatment. (C) H&E stains of RS4;11-LMC from same block as in A. Scale bar represents 25 μm, presented in the vehicle-treated group. (D) Representative images of D-luciferin bioluminescence in the same mice as in B. Images were taken prior to treatment (−2 h), and 28 and 48 h posttreatment. Timepoints for each image were chosen to allow washout of bioluminescent probe before subsequent imaging. (E) Relative levels of VivoGlo bioluminescence normalized to D-luciferin bioluminescence from individual animals. Data presented as mean ± SEM. *$P < 0.05$ versus vehicle group at the same timepoint.

damustine, as well as the combination regimen CHOP, were also evaluated in both the SC and systemic engraftment models. All of these treatments demonstrated significant inhibition of tumor growth and prolonged survival in the SC model (Table 1). However, only cyclophosphamide and the cyclophosphamide-containing regimen CHOP displayed significant delay in tumor growth in the systemic engraftment model. While response to CHOP

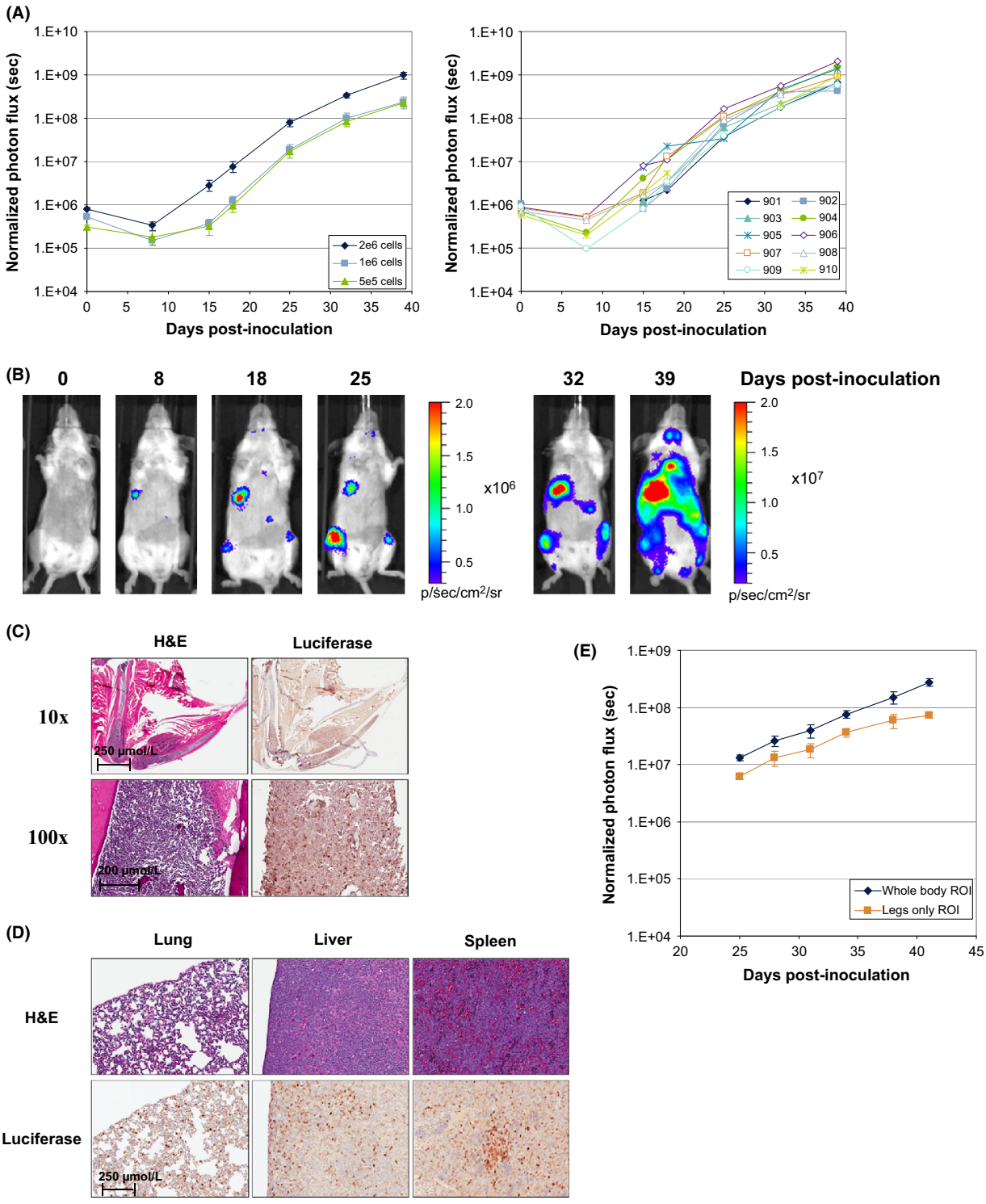

Figure 3. In vivo validation of RS4;11-LMC seeding following systemic inoculation. (A) Dose titration of RS4;11-LMC cells inoculated via the tail vein at 2×10^6, 1×10^6 and 5×10^5 cells/mouse. $N = 10$ mice per titration, data presented as mean BLI ± SEM. Graphs for the individual mice inoculated at 2×10^6 cells are shown. (B) Representative images from an individual mouse (#905) inoculated with 2×10^6 cells in A. (C) H&E and luciferase IHC staining in the leg of the RS4;11-LMC systemic engraftment model. (D) H&E and luciferase IHC staining in the lung, liver, and spleen of RS4;11-LMC systemic engraftment model. (E) Comparison of monitored growth rates of RS4;11-LMC using whole-body ROI or legs only ROI as the growth parameter.

was 4.8-fold less durable than in the SC model, durability of response to cyclophosphamide alone was equivalent in both models (Table 1).

Addition of Bcl-2 inhibitors enhances cyclophosphamide efficacy in the RS4;11-LMC systemic engraftment model

Using RS4;11-LMC systemically engrafted mice, we initially employed navitoclax to test the combination of Bcl-2 inhibition with cyclophosphamide, CHOP, and bendamustine. Combinations of navitoclax with cyclophosphamide containing regimens were more responsive than combinations with bendamustine (Table 1).

In a subsequent study, we tested cyclophosphamide in combination with navitoclax or venetoclax, using either one cycle of treatment or a second cycle after a 14 day drug holiday (Fig. 4B and C, respectively). By day 28, disease burden in the cyclophosphamide-treated group had relapsed and returned to the original size match levels. Tumors remained responsive to a second round of cyclophosphamide, although the level of regression and duration of response were both blunted compared to the first cycle of therapy. In the cyclophosphamide plus navitoclax or cyclophosphamide plus venetoclax groups, the combination induced a substantially greater regression, with a significant increase in tumor growth delay, relative to cyclophosphamide alone. The second cycle of the treatment maintained tumor regression throughout the second dosing period, while the single-regimen groups progressed to the endpoint. Representative images of individual mice in each treatment group are shown in Figure 4D.

Venetoclax and navitoclax, alone or in combination with cyclophosphamide, induce significant apoptosis in bone marrow tumors

To further test the ability of VivoGlo to detect apoptosis, we established RS4;11-LMC tumors in the bone marrow and treated the mice with venetoclax or navitoclax in combination with cyclophosphamide. Cleaved caspase induction is shown in Figure 5A. As with the flank tumors, venetoclax rapidly induced caspase activation, with 60% activation within 2 h, while both navitoclax and cyclophosphamide alone reached 60% within 24 h. Combination of Bcl-2 family inhibitors and cyclophosphamide increased both the extent and speed of caspase induction, with the venetoclax-cyclophosphamide combination reaching >90% after 2 h. By 24 h, quantification became difficult, with the necrosis in the bone marrow being difficult to distinguish from nascent marrow tissue in venetoclax-treated tumors, as shown in the H&E staining in Figure 5B. Percent cleaved caspase staining was estimated and plotted in Figure 5C. We repeated the experiments shown in Figure 2 with VivoGlo and D-luciferin in systemically engrafted mice; however, the bioluminescent signal was very weak resulting in low signal-to-noise ratios in these sites (Fig. S2).

Development of a systemic, bioluminescent MCL line with CNS penetrance

Systemic inoculation of Granta 519 cells induces disseminated disease leading to conspicuous clinical symptoms such as altered gait and loss of righting reflex (Ackler et al. 2012), which are suggestive of CNS impairment. Tracking

Table 1. Response rates of RS4;11-LMC in xenograft and systemic engraftment models to Bcl inhibitors and standard of care agents.

		SC xenograft		IV systemic		
Treatment	Dose (mg/kg per day)	Schedule	%TGD[1]	Schedule	%TGD[1]	%TGD[1] (+navit)
Navitoclax	100	p.o. q.d. × 7	>133[3]	p.o. q.d. × 14	57[3]	N/A
Venetoclax	100	p.o. q.d. × 7	>133[3]	p.o. q.d. × 14	67[3]	N/A
Cyclophosphamide	100	i.p. q.4d. × 4	127[3]	i.p. q.4d. × 4	136[3]	200[4]
Cyclophosphamide[2]	25	i.p. q.d. × 1	67[3]	i.p. q.d. × 1	14[3]	86[4]
Doxorubicin	3	i.v. q.d. × 1		i.v. q.d. × 1		
Vincristine	0.25	i.v. q.d. × 1		i.v. q.d. × 1		
Prednisolone	0.5	p.o. q.d. × 1		p.o. q.d. × 1		
Bendamustine	25	i.v. q.d. × 1	19[3]	i.v. q.d. × 1	0	57
	25	i.v. q.7d. × 2	29[3]	i.v. q.7d. × 2	−6	46[4]

[1]% Tumor growth delay.
[2]Representative of CHOP. All four agents administered on d1, spaced 90 min apart in order shown.
[3]$P < 0.05$ versus vehicle control (Kaplan–Meier log rank test).
[4]$P < 0.05$ versus cytotoxic(s) (Kaplan–Meier log rank test).

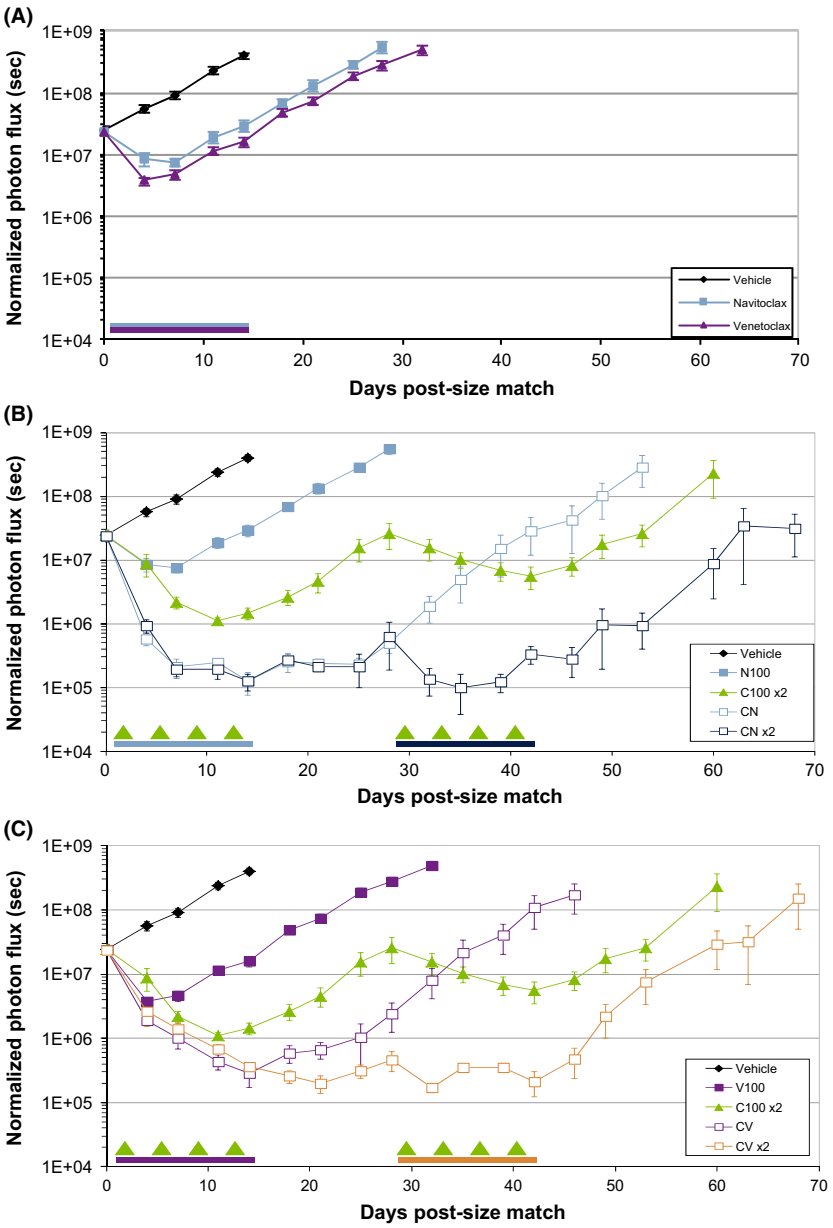

Figure 4. Combination activity of Bcl-2 inhibitors with cyclophosphamide in the RS4;11-LMC systemic engraftment model. (A) Efficacy of either vehicle, navitoclax,or venetoclax (100 mg·kg^{-1}·day^{-1}, p.o. q.d. × 14) as monitored ventrally by longitudinal whole-body ROI. Blue and purple bars represent navitoclax and venetoclax dosing period, respectively. (B) Response of RS4;11-LMC systemic engraftment model to repeated cycle of cyclophosphamide (100 mg·kg^{-1}·day^{-1}, i.p. q.4d. × 4; C100 × 2) or cyclophosphamide plus navitoclax (mg·kg^{-1}·day^{-1}, p.o. q.d. × 14) through one (CN) or two (CN × 2) cycles, as monitored ventrally by longitudinal whole-body ROI. (C) Response of RS4;11-LMC systemic engraftment model to repeated cycle of cyclophosphamide (100 mg·kg^{-1}·day^{-1}, i.p. q.4d. × 4, C100 × 2) or cyclophosphamide plus venetoclax (100 mg·kg^{-1}·day^{-1}, p.o. q.d. × 14) through one (CV) or two (CV × 2) cycles, as monitored ventrally by longitudinal whole-body ROI. Data presented as mean ± SEM. For all experiments, arrows represent cyclophosphamide dosing days, color-coded bars represent relevant Bcl-2 family inhibitor dosing periods. (D) Representative images of mice from each treatment group presented above.

engraftment and disease progression in mice following IV inoculation of Granta 519-LMC cells revealed consistent infiltration and replacement of bone marrow in long bones with extension to the surrounding skeletal muscle similarly to RS4;11-LMC (Fig. 6A and B). Granta 519-LMC also affected medullary trabecular bones and cortical compact bones. Bioluminescent images revealed spinal infiltration in most mice, with subsequent brain involvement in a smaller percentage of animals. Growth rate of tumor as monitored by BLI was similar from both the dorsal and

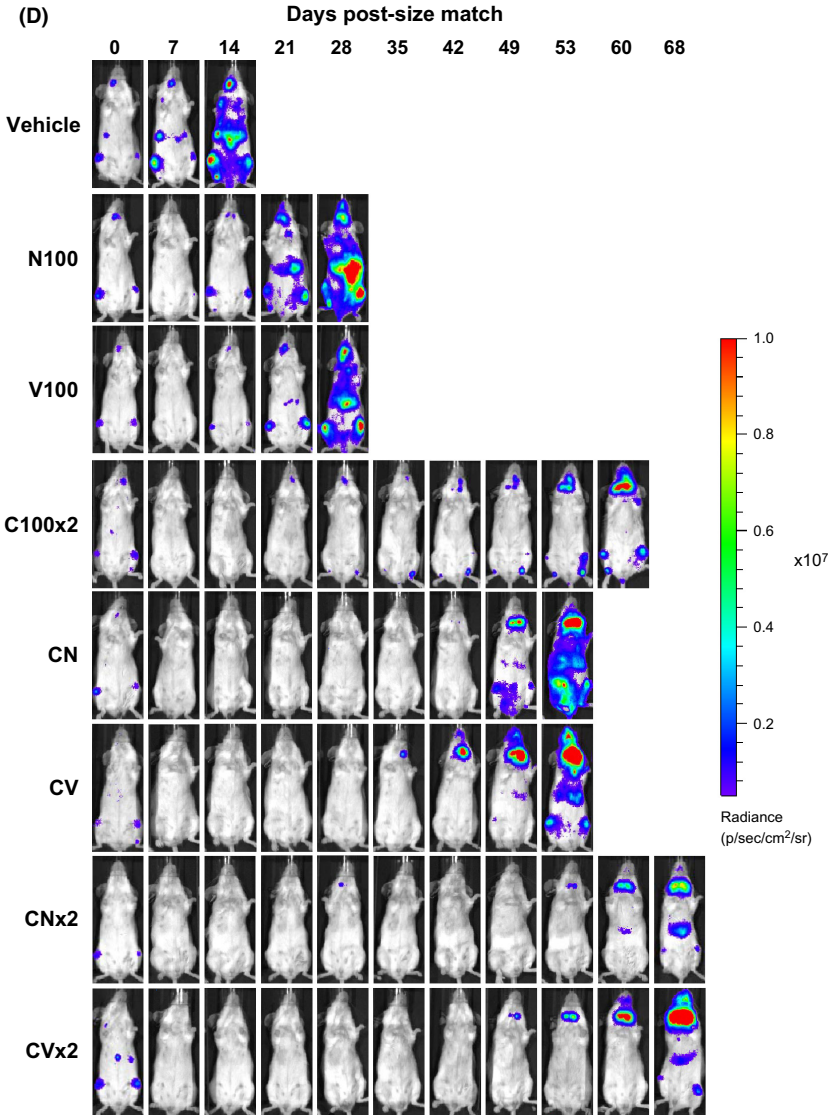

Figure 4. Continued.

ventral positions (Fig. 6C). Histological analysis (H&E) of spinal cords revealed multifocal infiltration of tumor cells with disruption of their normal architecture. Adjacent neuronal tissues showed a large number of vacuoles (spongiosis) with degeneration and necrosis of several neurons. IHC analysis of vertebral and long bone sections confirmed the presence of luciferase-expressing cells in the respective bone marrow and spinal cord (Fig. 6D).

Addition of Bcl-2 inhibitors enhances BR efficacy in the Granta 519-LMC systemic engraftment model

To monitor the response of CNS infiltrates into BR and navitoclax, or venetoclax, Granta 519-LMC was inoculated into mice and size-matched at 14 days post-inoculation based on dorsal whole-body ROI. Neither navitoclax nor venetoclax demonstrated single agent activity (Fig. 7A). BR alone led to regression in this model, which rebounded approximately 10 days after treatment. Addition of either navitoclax or venetoclax to BR induced a deeper and more rapid regression in tumor burden, and approximately doubled the delay in tumor regrowth as compared to BR alone. Representative images of individual mice are shown for each treatment group (Fig. 7B). Importantly, bioluminescent signal in the spinal column was reduced with combination therapy, demonstrating that Granta 519 cells which penetrate the CNS can be accessed and respond to Bcl-2 family inhibitors and BR (Fig. 7B, Fig. S3).

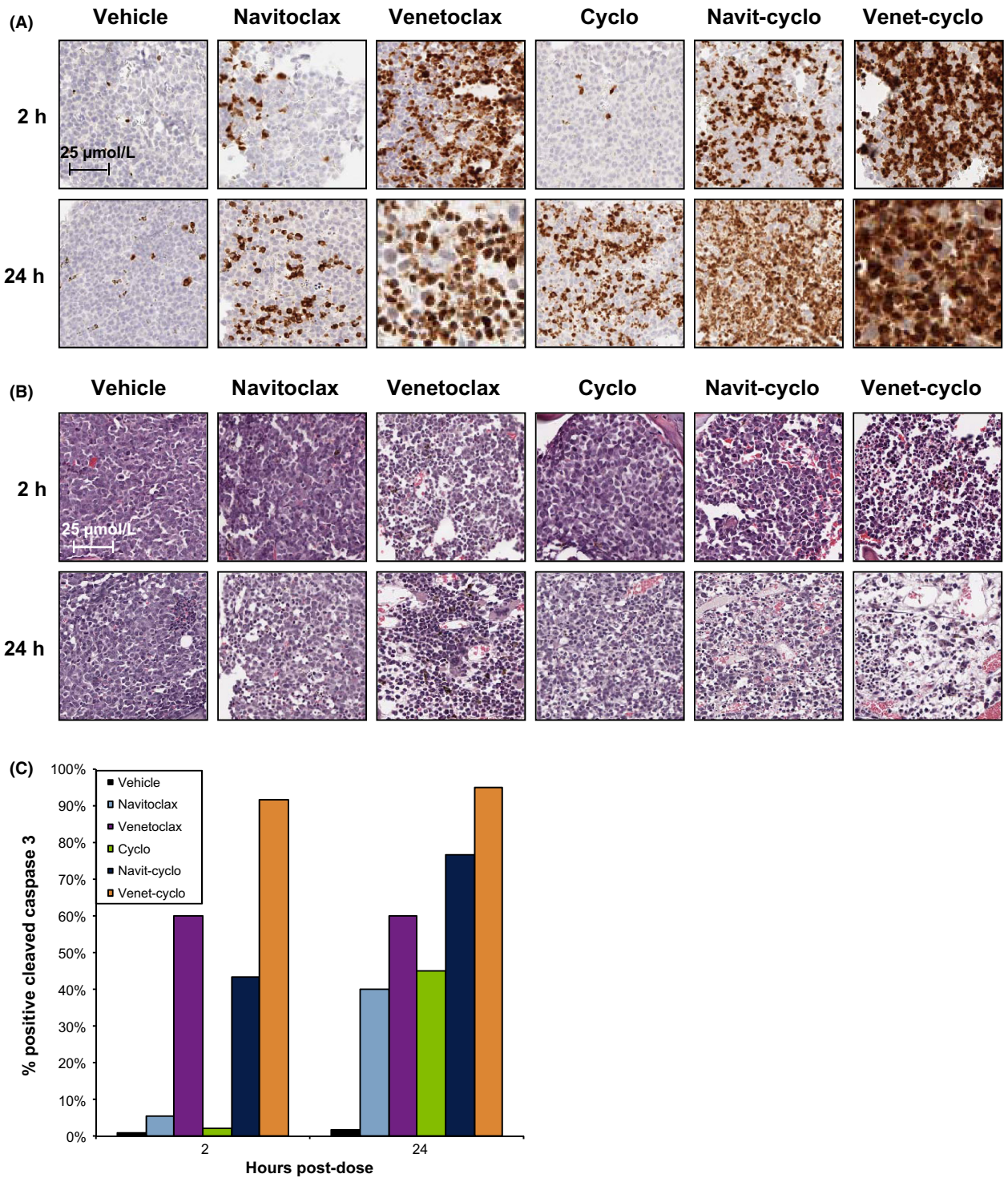

Figure 5. Activation of caspase 3 and cell killing in RS4;11 systemic engraftment tumors following treatment with cyclophosphamide and/or navitoclax or venetoclax. (A) Staining for cleaved caspase-3/7 in RS4;11-LMC bone marrow sections following a single dose of navitoclax, venetoclax, or cyclophosphamide (cyclo)(100 mg·kg^{-1}), or a combination of cyclophosphamide and navitoclax (navit-cyclo) or venetoclax (venet-cyclo). Pictures are representative images for each timepoint (N = 3). (B) H&E stains of RS4;11-LMC from same block as in A. Scale bar represents 25 μm, presented in the 2 h vehicle-treated group. (C) Quantitation of caspase staining in A. Error bars are not provided, since this was a visual score by a trained pathologist.

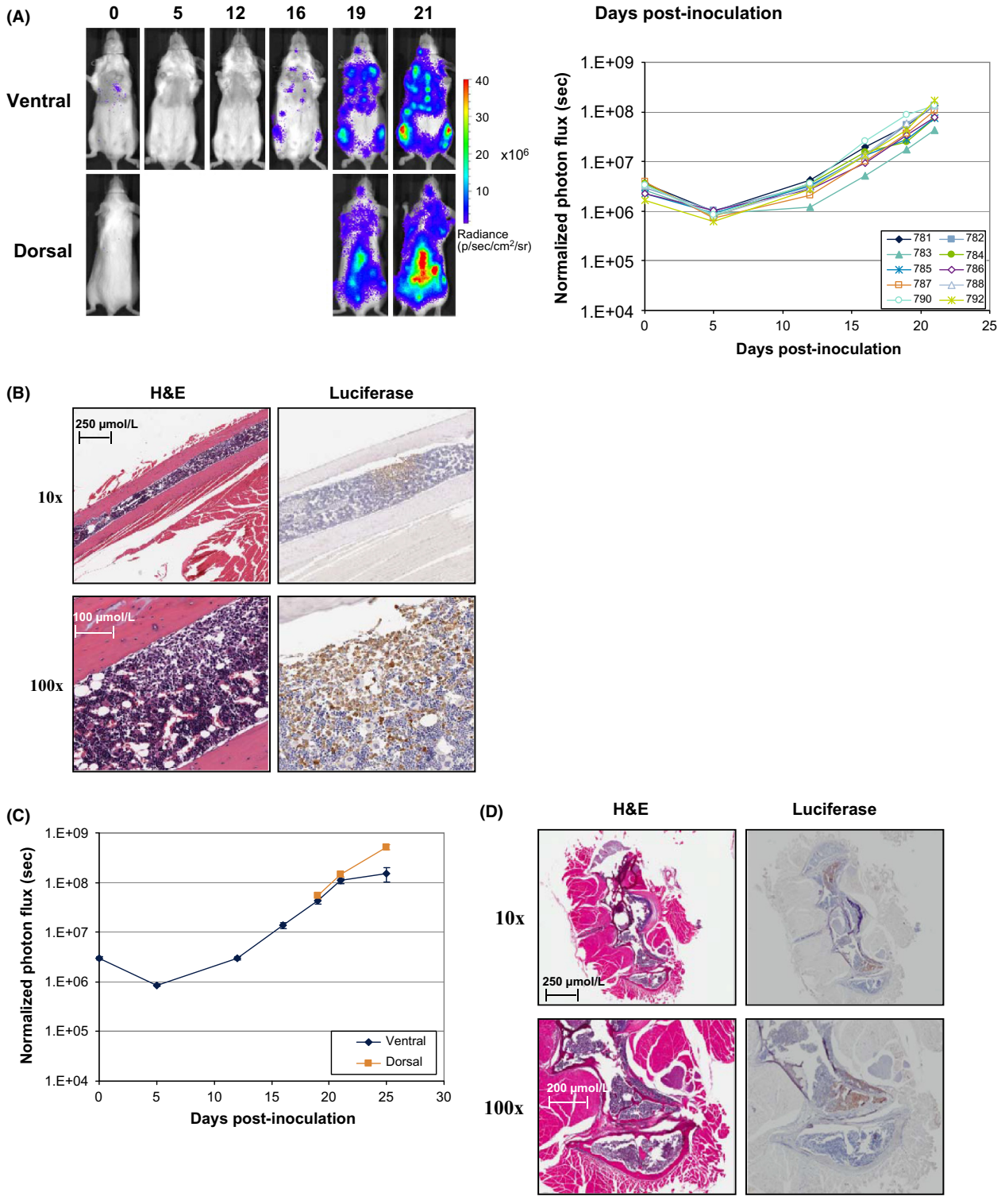

Figure 6. In vitro and in vivo characterization of Granta 519-LMC. (A) Growth rate of Granta 519-LMC cells inoculated via the tail vein at 5×10^6 cells · mouse^{-1}. Graphs for the ventral images of individual mice are shown. $N = 10$ mice. Representative dorsal and ventral images from an individual mouse (#788). (B) H&E and luciferase IHC staining in a longitudinal section of the long bone of a mouse systemically inoculated with Granta 519-LMC (10x and 100x). (C) Dorsal versus ventral BLI following size match of Granta 519-LMC. (D) H&E and luciferase IHC staining in a longitudinal section of vertebral column of a mouse systemically inoculated with Granta 519-LMC (10x and 100x).

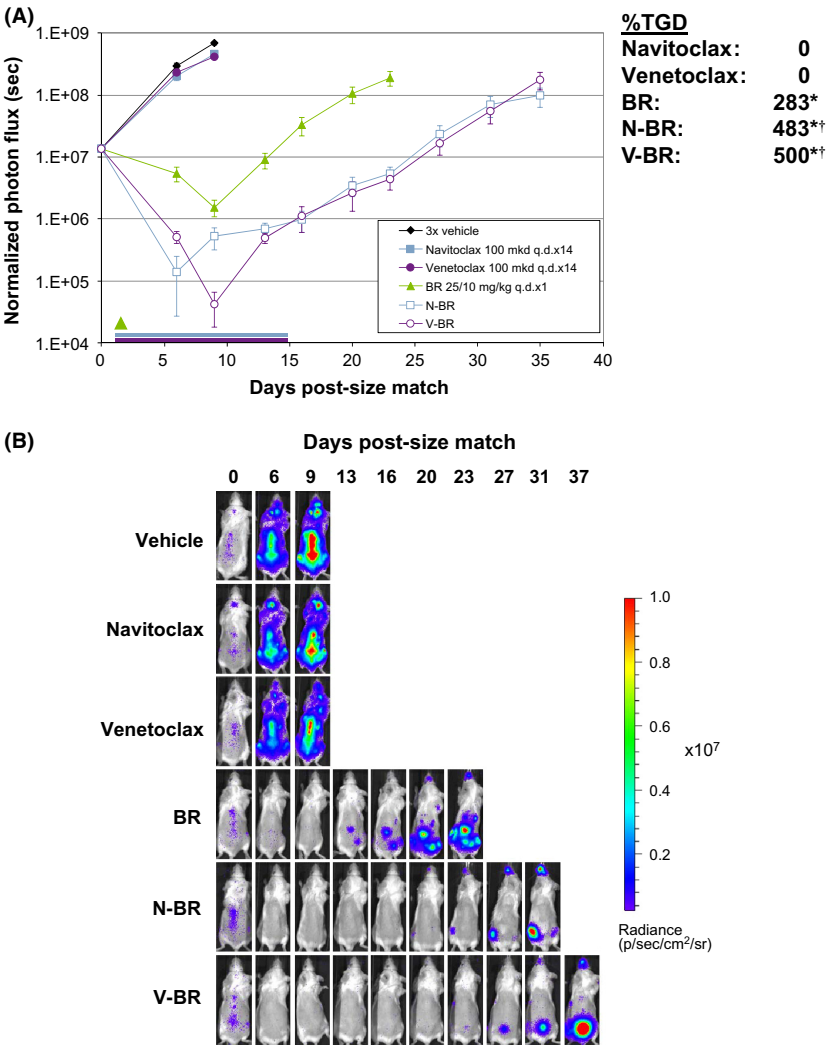

Figure 7. Combination activity of Bcl-2 inhibitors with BR in the systemic Granta 519-LMC model. (A) Combination activity of BR (25/10 mg·kg^{-1}, i.v. q.d. × 1) and navitoclax or venetoclax (100 mg·kg^{-1}·day^{-1}, p.o. q.d. × 14). Graphs represent dorsal measurements to capture brain and spinal responses. Green arrow represents BR administration, blue and purple bars represent navitoclax and venetoclax dosing period, respectively. Inset shows %TGD values for each treatment group. (B) Representative images of mice treated with BR and/or navitoclax or venetoclax. Data presented as mean BLI ± SEM. *P < 0.05 versus vehicle. †P < 0.05 versus BR monotherapy.

Discussion

We demonstrate herein that the LMC-labeled ALL cell line RS4;11 engraft within the bone marrow, liver, lung, and spleen, and that growth of these tumors can be readily tracked longitudinally by bioluminescent imaging. Additionally, the MCL cell line Granta 519-LMC engrafts primarily in the CNS, most often in the extra and intradural space of the spinal column, as well as the bone marrow. Engraftment and growth in distal sites was consistent and reproducible across animals. Importantly, bone engraftment did not require the use of more permissive animal strains (i.e., NSG or NOD/SCID mice), or preconditioning of the host with irradiation to eliminate existing marrow, improving survival rates prior to size match. Following development of these models, we then demonstrated therapeutic efficacy of standard-of-care chemotherapeutics as well as the Bcl-2 small molecule inhibitors, venetoclax and navitoclax.

Clinically, leukemias preferentially localize to the bone marrow compartment, where they are more resistant to apoptosis induction (Chiorazzi et al. 2005). Vogler et al. (2009) and Butterworth et al. (2009) have demonstrated that primary chronic lymphocytic leukemia (CLL) cells become resistant to the navitoclax-related inhibitor ABT-737 when cocultured in vitro with stromal cells found in lymph nodes or bone marrow. Data presented

here, however, demonstrate that RS4;11-LMC cells within bone marrow and other tissues remain responsive to both navitoclax and venetoclax (Fig. 4), although the response was less durable than in the SC model. Similarly, navitoclax and venetoclax have been reported to significantly decrease splenomegaly, as well as nodal and marrow load as a single agent, in CLL and NHL patients, respectively (Wilson et al. 2010; Davids et al. 2012; Roberts et al. 2012). While the reason for this discrepancy is unclear, a likely explanation is the natural in vivo environment of lymph nodes and bone marrow are not accurately reproduced in these coculture systems.

CNS involvement with non-Hodgkin's lymphoma is associated with poor prognosis and significant increased mortality (Gill et al. 2009), yet the mechanism by which CNS invasion occurs and the progression therein are poorly understood. MCL is known to invade the CNS in a low percentage of cases, particularly after relapse and when presenting with high-risk factors, such as a blastoid phenotype (Gill et al. 2009). One important observation was seeding of Granta 519-LMC in the CNS, consistent with the fact that the parent cell line was established from a patient whose disease was blastoid in phenotype whom had rapidly relapsed following therapy (Jadayel et al. 1997). To the best of our knowledge, this is the first report of a preclinical MCL model using a bioluminescent reporter for noninvasively monitoring engraftment and disease progression in the CNS. Furthermore, these data demonstrate that Bcl-2 family inhibitors navitoclax or venetoclax plus BR are capable of accessing Granta 519-LMC CNS lesions and provide significant antitumor efficacy.

Navitoclax was developed for single-agent therapy of hematologic malignancies. Venetoclax supplanted navitoclax because of its higher potency coupled with the lack of Bcl-x_L inhibition making it platelet sparing (Souers et al. 2013). As shown in Figure 1C, venetoclax and navitoclax appear roughly equivalent in their ability to regress RS4;11 SC tumors after repeated dosing. However, in agreement with clinical data, we observed increased in vivo potency of venetoclax following a single dose as measured by immunohistochemistry for caspase 3 cleavage. Approximately, 70% of venetoclax-treated tumor mass stained positive for cleaved caspase 3 after 2 h of treatment, as compared to approximately 5% for navitoclax-treated tumors. This increase in apoptosis correlated with a faster induction of tumor cell necrosis (35% by 2 h, 99% by 24 h) than with navitoclax (5% by 2 h, 80% by 24 h). Furthermore, increased potency of venetoclax was independently confirmed noninvasively by molecular imaging with the activatable bioluminescent apoptosis probe VivoGlo normalized to cell viability (D-luciferin). In the systemic model, similar results were obtained revealing faster caspase 3 activation in the bone marrow compartment with venetoclax (60% by 2 h) than with navitoclax (5% by 2 h). Such rapid induction of apoptosis and concomitant decrease in viable cells within the tumor following treatment more accurately reflects the clinical response of patients during phase 1 trials with venetoclax (Souers et al. 2013), where tumor lysis syndrome was more prevalent with venetoclax, but suggest that over time navitoclax leads to similar tumor cell killing.

In the RS4;11 systemic model, VivoGlo probe was assessed, but we were unable to detect specific bioluminescent signal over the background in treated animals (Fig. S2). This limitation in probe utility is likely due to the presence of fewer cancer cells and greater tissue penetration requirements compared to the SC model. An additional limitation of both RS4;11 and Granta 519 systemic models is the requirement of immunocompromised mice for xenografting, thereby eliminating the ability to monitor host immune cell interactions with tumor cells. A similar approach as the one we outlined here transducing murine leukemia and/or lymphoma cancer cell lines with a bioluminescent reporter could enable allograft-inglabeled cancer cells in immune competent mice, allowing the role of the functional immune cells and/or immunomodulatory agents to be analyzed.

In conclusion, we demonstrate that venetoclax and navitoclax are effective at regressing tumors from leukemia and lymphoma cells in distal sites, including bone marrow and the CNS, and combination therapy was effective at enhancing this response. Results in systemic models were more predictive of clinical results than SC xenografts (Roberts et al. 2012; Davids et al. 2013; Seymour et al. 2013), and these models provide a powerful system for preclinical evaluation of chemotherapeutic agents.

Acknowledgements

The authors thank Gary Chiang for critical review of the manuscript.

Author Contributions

A Oleksijew, J Chen, BJ Chyla, J Clarin, K Foster, T McGonigal, S Schlessinger, ML Smith, SK Tahir and J Hickson performed the research.

S Ackler, JD Leverson, AJ Souers, ER Boghaert and J Hickson designed the research study.

S Ackler, S Mishra and J Hickson analyzed the data.

S Ackler, JD Leverson, AJ Souers, ER Boghaert, and J Hickson wrote the paper.

Disclosures

All authors are employees of AbbVie. This study was sponsored by AbbVie. AbbVie contributed to the study design, research and interpretation of data, writing, reviewing, and approving the publication.

References

Ackler S, Mitten MJ, Foster K, Oleksijew A, Refici M, Tahir SK, et al. (2010). The Bcl-2 inhibitor ABT-263 enhances the response of multiple chemotherapeutic regimens in hematologic tumors in vivo. Cancer Chemother Pharmacol 66: 869–880.

Ackler S, Mitten M, Chen J, Clarin J, Foster K, Jin S, et al. (2012). Navitoclax (ABT-263) and bendamustine +/- rituximab induce enhanced killing of non-Hodgkin's lymphoma tumours in vivo. Br J Pharmacol 167: 881–891.

Butterworth M, Vogler M, Dyer MJ, Cohen GM (2009). Response: microenvironment-dependent resistance to ABT-737 in chronic lymphocytic leukemia. Blood 114: 2561.

Chiorazzi N, Rai KR, Ferrarini M (2005). Chronic lymphocytic leukemia. N Engl J Med 352: 804–815.

Davids MS, Roberts AW, Anderson MA, Pagel JM, Kahl BS, Gerecitano JF, et al. (2012). The Bcl-2-specific BH3-mimetic ABT-199 (GDC-0199) is active and well-tolerated in patients with relapsed non-Hodgkin lymphoma: interim results of a phase I study. Blood (ASH Annual Meeting Abstracts) 120: a304.

Davids MS, Seymour JF, Gerecitano JF, Kahl BS, Pagel JM, Wierda WM, et al. (2013) The Bcl-2 inhibitor ABT-199 (GDC-0199) is active and well tolerated in patients with relapsed/refractory mantle cell lymphoma and other non-Hodgkin's lymphomas. EHA Congress Abstracts P849.

Gill S, Herbert KE, Prince HM, Wolf MM, Wirth A, Ryan G, et al. (2009). Mantle cell lymphoma with central nervous system involvement: frequency and clinical features. Br J Haematol 147: 83–88.

Hickson J (2009). In vivo optical imaging: preclinical applications and considerations. Urol Oncol 27: 295–297.

Hickson J, Ackler S, Klaubert D, Bouska J, Ellis P, Foster K, et al. (2010). Noninvasive molecular imaging of apoptosis in vivo using a modified firefly luciferase substrate, Z-DEVD-aminoluciferin. Cell Death Differ 17: 1003–1010.

Jadayel DM, Lukas J, Nacheva E, Bartkova J, Stranks G, de Schouwer PJ, et al. (1997). Potential role for concurrent abnormalities of the cyclin D1, p16CDKN2 and p15CDKN2B genes in certain B cell non-Hodgkin's lymphomas. Functional studies in a cell line (Granta 519). Leukemia 11: 64–72.

Kaijzel EL, van der Plujim G, Lowik CW (2007). Whole-body optical imaging in animal models to assess cancer development and progression. Clin Cancer Res 13: 3490–3497.

Kilkenny C, Browne W, Cuthill IC, Emerson M, Altman DG (2010). NC3Rs Reporting Guidelines Working Group. Br J Pharmacol 160: 1577–1579.

Liem NL, Papa RA, Milross CG, Schmid A, Tajbakhsh M, Choi S, et al. (2004). Characterization of childhood acute lymphoblastic leukemia xenograft models for the preclinical evaluation of new therapies. Blood 103: 3905–3914.

Lock R, Carol H, Houghton PJ, Morton CL, Kolb EA, Gorlick R, et al. (2008). Initial testing (stage 1) of the BH3 mimetic ABT-263 by the pediatric preclinical testing program. Pediatr Blood Cancer 50: 1181–1189.

McGrath J, Drummond G, Kilkenny C, Wainwright C (2010). Guidelines for reporting experiments involving animals: the ARRIVE guidelines. Br J Pharmacol 160: 1573–1576.

O'Neill K, Lyons SK, Gallagher WM, Curran KM, Byrne AT (2010). Bioluminescent imaging: a critical tool in pre-clinical oncology research. J Pathol 220: 317–327.

Park CM, Bruncko M, Adickes J, Bauch J, Ding H, Kunzer A, et al. (2008). Discovery of an orally bioavailable small molecule inhibitor of prosurvival B-cell lymphoma 2 proteins. J Med Chem 51: 6902–6915.

Roberts AW, Seymour JF, Brown JR, Wierda WG, Kipps TJ, Khaw SL, et al. (2012). Substantial susceptibility of chronic lymphocytic leukemia to BCL2 inhibition: results of a phase I study of navitoclax in patients with relapsed or refractory disease. J Clin Oncol 30: 488–496.

Sekiguchi N, Kobayashi Y, Yokota Y, Kusumoto S, Tanimoto K, Watanabe T, et al. (2005). Follicular lymphoma subgrouping by fluorescence in situ hybridization analysis. Cancer Sci 96: 77–82.

Seymour JF, Davids MS, Pagel JM, Kahl BS, Wierda WG, Miller TP, et al. (2013). Bcl-2 inhibitor ABT-199 (GDC-0199) monotherapy shows anti-tumor activity including complete remissions in high-risk relapsed/refractory (R/R) chronic lymphocytic leukemia (CLL) and small lymphocytic lymphoma (SLL). Blood (ASH Annual Meeting Abstracts) 122: a872.

Souers AJ, Leverson JD, Boghaert ER, Ackler SL, Catron ND, Chen J, et al. (2013). ABT-199, a potent and selective BCL-2 inhibitor, achieves antitumor activity while sparing platelets. Nat Med 19: 202–208.

Tse C, Shoemaker AR, Adickes J, Anderson MG, Chen J, Jin S, et al. (2008). ABT-263: a potent and orally bioavailable Bcl-2 family inhibitor. Cancer Res 68: 3421–3428.

Tsujimoto Y, Finger LR, Yunis J, Nowel PC, Croce CM (1984). Cloning of the chromosome breakpoint of neoplastic B cells with the t(14;18) chromosome translocation. Science 226: 1097–1099.

Vogler M, Butterworth M, Majid A, Walewska RJ, Sun XM, Dyer MJ, et al. (2009). Concurrent up-regulation of BCL-x_L and BCL2A1 induces approximately 1 000-fold resistance to

ABT-737 in chronic lymphocytic leukemia. Blood 113: 4403–4413.

Wei MC (2004). Bcl-2-related genes in lymphoid neoplasia. Int J Hematol 80: 205–209.

Weissleder R, Pittet M (2008). Imaging in the era of molecular oncology. Nature 452: 580–589.

Wilson WH, O'Connor OA, Czuczman MS, LaCasce AS, Gerecitano JF, Leonard JP, et al. (2010). Navitoclax, a targeted high-affinity inhibitor of BCL-2, in lymphoid malignancies: a phase I dose-escalation study of safety, pharmacokinetics, pharmacodynamics, and antitumour activity. Lancet Oncol 11: 1149–1159.

Supporting Information

Additional Supporting Information may be found in the online version of this article:

Figure S1. Chemical structure of navitoclax (ABT-263) and venetoclax. Marked atom represents chiral center of navitoclax.

Figure S2. In vivo imaging of VivoGlo in RS4;11 systemic engraftment tumors. Images of mice-bearing systemically engrafted RS4;11-LMC tumors 2 h following a single dose of either vehicle or venetoclax plus cyclophosphamide. Mice were imaged using either D-luciferin predose (−2 h) or VivoGlo (2 h).

Figure S3. Individual images of early time points demonstrating addition of Bcl-2 inhibitors enhances BR efficacy in the Granta 519 LMC systemic engraftment model. Images of all individual mice (n = 8 per group) at early time points in BR-containing dosing regimens. Imaging thresholds (minimum and maximum) have been adjusted uniformly across all images to demonstrate CNS engraftment of Granta 519 LMC cells prior to therapy and subsequent rapid regression in response to treatment.